CHEMISTRY OF MATERIALS

pubs.acs.org/cm

Article

Interpretation of Oxygen 1s X-ray Photoelectron Spectroscopy of ZnO

Terry J. Frankcombe* and Yun Liu*

Cite This: https://doi.org/10.1021/acs.chemmater.3c00801

Read Online

ACCESS | Metrics & More | Article Recommendations | Supporting Information

ABSTRACT: X-ray photoelectron spectroscopy (XPS) is widely used to determine the chemical and electronic states of atoms within a material. However, it is often complex to interpret the O 1s region in metal oxides, where an ~531 eV binding energy feature appears between lattice oxygen (~530 eV) and oxygen-containing surface species (~532 eV). This feature has been vaguely ascribed to oxygen vacancies or oxygen deficient regions for many decades. This work employs full-potential density functional theory to calculate the binding energies of the O 1s electrons under two- and three-dimensional periodic boundary conditions as a probe of expected XPS spectra. ZnO is used as an example system. Both bulk crystal regions containing a range of oxygen defects and slabs with a range of surface terminations and functionalizations have been considered. The slabs considered are mostly $\{10\bar{1}0\}$ and $\{11\bar{2}0\}$ surfaces that are not expected to be reconstructed from the cleaved bulk structure. The resulting O 1s binding energies show no signature for oxygen defects in bulk regions. Furthermore, the 531 eV binding energy feature often ascribed to oxygen vacancies or oxygen deficient regions can instead be readily explained by the O 1s electrons from water molecules strongly bound to the exposed ZnO surface (i.e., chemisorbed, as distinct from more loosely bound water) or surface oxygen passivated with hydrogen. This work will rectify many misinterpretations of XPS data of the O 1s region in metal oxides, provide guidance for precisely understanding the oxygen states of a material, and subsequently enable the real origin of material properties to be revealed.

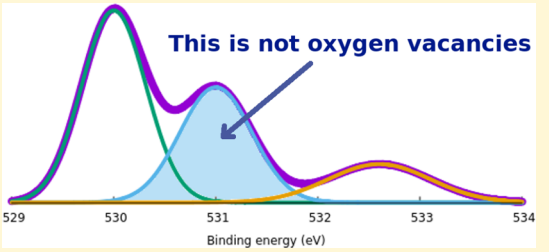

1. INTRODUCTION

X-ray photoelectron spectroscopy (XPS)[1] is a powerful technique for analyzing the elemental composition of materials, yielding information about chemical environments, oxidation states, etc. It is a surface sensitive technique that probes at most tens of nanometers into a material surface, depending on the elements involved.

XPS readily reveals the presence of oxygen in a material. Oxygen species usually generate at least two peaks in the XPS photoelectron binding energy spectrum, one for bulk or lattice O and one for oxygen bound to the surface. However, the observed XPS spectrum is often decomposed into more than two components. Often a component that is associated with "oxygen vacancies" is ascribed to features that can be either observed or fit to a third Voigt peak that lies between the lattice oxygen peak (with a binding energy of ~530 eV) and the adsorbed species peak (typically ~532 eV). A distinct XPS signal corresponding to a binding energy of 531 eV is regularly ascribed to "oxygen vacancies".

An analysis of the literature (see section 1 of the Supporting Information) reveals that assigning an O 1s XPS peak around 531 eV to oxygen vacancies or "oxygen deficient regions" originates in the work of the highly respected materials chemist (later Nobel laureate) John C. Goodenough and his colleague John C. C. Fan, published in 1977.[2] Fan and Goodenough used XPS to study pure and Sn-doped In_2O_3. In that work, the O 1s XPS peaks could be decomposed into a sum of two overlapping Gaussian functions, centered at 529.9 and 531.6 eV. Apparently on the basis of observations of oxygen in the mixed cation valence compound Co_3O_4, Fan and Goodenough concluded that one of these signals came from oxygen ions adjacent to O-saturated In ions and the other from oxygen ions adjacent to In ions with oxygen vacancies in their coordination shell.

There are some problems with the interpretation of the 531 eV signal by Fan and Goodenough. First, an unsaturated environment should destabilize the electronic structure and give lower binding energies than the binding energy of 530 eV that comes from well-matched ionic environments, not the more stable electrons required for the higher 531 eV binding energy. The original argument by Fan and Goodenough was based on a multivalence argument even though they stated explicitly that the In oxidation states did not vary.[2] Fan and Goodenough further suggested that the binding energy of O 1s electrons should change depending on the vacancy concentration.

Received: April 5, 2023
Revised: June 13, 2023

Subsequent authors have not generally commented on this, considering only changes in the intensity of 531 eV emission as being indicative of changes to the vacancy concentration. There is another unaddressed question. If the 531 eV signal comes from regions that are oxygen deficient but not sufficiently so to yield formal oxidation state changes of the cations, how could this result in a single shell of discretely altered binding energies and not a range of binding energies as the influence of the presumed vacancies wanes with distance? Finally, as has recently been explicitly mentioned,[3] there are no core electrons present in an oxygen vacancy to be emitted upon absorption of an X-ray photon, although this does not preclude the supposition of an effect on the oxygens in the vicinity of an oxygen vacancy (the "oxygen deficient region").

This 45-year-old assignment, based on the high level of oxygen vacancies in synthesized In_2O_3, is widely used throughout the study of oxide materials. Given the problems that can be identified with the underpinnings of the assignment, it is past time to look for independent corroboration. In this work, we use computational methods to investigate the core state electrons that give rise to the O 1s spectrum and search for correlations between simulated structures and these O 1s energy levels. We chose ZnO as our target material. ZnO has a reasonably simple wurtzite crystal structure and is widely reported to yield three O 1s XPS features. The low- and high-binding energy features are usually attributed to lattice oxygen and surface species, while the intermediate-energy feature, ∼1 eV above the binding energy of the lattice oxygen binding energy, is almost universally assigned following Fan and Goodenough to oxygen deficient regions.[4−29]

2. METHODS

In this work, we use density functional theory (DFT) to evaluate the electronic structure of ZnO. As we are primarily interested in core electronic states, a full-potential method is required. This work primarily uses the full-potential linearized augmented plane wave (FLAPW) method[30−32] as implemented in the open-source FLEUR code.[33,34]

All calculations were performed using the PBE functional.[35] Most computational parameters were left at the FLEUR defaults. Exceptions are the maximum atomic basis angular momentum quantum number cutoffs l^{α}_{max} and $l^{\alpha}_{nonspher}$ were increased to 14 and 8, respectively, for Zn ions and 8 and 6, respectively, for O and H. In cases in which this did not present an excessive computational burden (that is, for all calculations except bulk supercell calculations), the plane wave and reciprocal space cutoffs K_{max}, G_{max}, and G^{xc}_{max} were increased to 5.8, 15.1, and 14.3 a_0^{-1}, respectively.

The muffin-tin radii were taken to be 2.18 a_0 for Zn, 0.97 a_0 for O, and 0.94 a_0 for H.

In all FLAPW calculations, the atomic positions were allowed to relax until the Cartesian components of all forces were $<10^{-3}$ E_h/a_0.

The initial state approximation, in which we take binding energies to be represented by the energies of the occupied core orbitals, was used throughout.[36,37] Thus, screening effects are ignored. However, we can expect screening effects to be small compared to the ∼1 eV shift between the 530 and 531 eV XPS features we seek.[38] Furthermore, we expect screening effects to largely be canceled out by the lattice oxygen shift that is applied, as described below.

3. RESULTS

3.1. XPS of Defects in the Bulk. For a single ZnO unit cell, the optimized structure (space group #186, $P6_3mc$) was found to have lattice parameters a = 3.2891 Å and c = 5.3068 Å, with Zn ions at the 2b site with coordinates of ($^1/_3$, $^2/_3$, 0) and O ions at the 2b site with coordinates of ($^1/_3$, $^2/_3$, 0.3792).

The O 1s energy level for this optimized structure was calculated to be ∼505 eV below the calculated Fermi level. This is clearly different from the observed binding energy from XPS of ∼530 eV. An absolute energy level offset like this is expected from such a calculation.[39] Such uncertainty in the calculated energy levels will be exacerbated when we later look at ZnO surfaces, in which the surface work function plays a role as the work function changes with changes in the details of the exposed surface. What can be considered reliable is the relative energies of different core states. Thus, in the context of this work, we are looking for O 1s states that lie 1−2 eV lower in energy than these 1s states of the lattice oxygen ions. To that end, in this work, we present all subsequent O 1s energy levels shifted so that the lattice oxygen falls at exactly 530 eV. While a 530 eV base for lattice oxygen is appropriate for ZnO, note that less ionic oxides exhibit higher binding energies for the O 1s electrons.

A 3 × 3 × 2 supercell of the ZnO unit cell was constructed, and one oxygen atom removed. The O 1s energy levels of the 1s atoms were examined after ionic relaxation.

Taking the 1s energy level of an oxygen ion far (>8 Å) from the vacancy as the reference energy, we find the lowest calculated O 1s energy levels lie only 0.06 meV lower in energy. That is, if we pin the 1s binding energy of lattice oxygen at exactly 530 eV, the 1s binding energies of oxygen ions near an oxygen vacancy, as probed by XPS, are calculated to be 530.06 eV (noting that shifting the O 1s level to a lower energy increases the binding energy relative to vacuum). Such core states would be indistinguishable from the nondefective lattice oxygen in an XPS measurement. These calculations do not support the XPS feature that appears at a binding energy of ∼531 eV to be related to oxygen lattice vacancies.

We similarly investigated a number of different structures with oxygen-related defects (including some that might be considered unlikely) in an effort to find oxygen-defective structures that might explain the XPS signal at 531 eV. Adding neutral interstitial oxygen induced 1s binding energy shifts from 0.17 to −0.10 eV. Combining a vacancy with an interstitial oxygen in a separated Frenkel defect had the strongest impact on the calculated energy levels, but in the wrong direction as the binding energy was decreased by 1.8 eV. The largest increase in the calculated O 1s binding energy was found to be for added interstitial OH, where the O 1s energy level shifted by <0.5 eV, short of the ≥1 eV difference usually observed between the 530 and 531 eV XPS peaks. These DFT calculations do not support the notion that the 531 eV XPS peak arises from "oxygen vacancies or oxygen deficient regions".

3.2. Bare ZnO Surfaces. If the XPS peak at 531 eV does not come from oxygen vacancy regions, we need to look for another explanation. The discrete peak often observed at 532 eV or a higher binding energy is usually ascribed to the oxygen-containing species on the crystal surface. We can examine the XPS signals expected from oxygen-containing surface structures and moieties to determine whether DFT calculations support this interpretation and if the 531 eV peak might be from a surface structure.

To calculate O 1s energy levels for oxygens in surface structures, we need to construct slabs exposing relevant ZnO crystal surfaces. In this section, we examine some relevant low-index surfaces of ZnO.[40−42]

Figure 1 illustrates the {0001}, {10$\bar{1}$0}, and {11$\bar{2}$0} surfaces of ZnO, created by cleavage of the pure crystal and relaxation of the ion positions of the slab. (Note that the FLEUR code used in this work allows the consideration of two-dimensional periodic slabs,

https://doi.org/10.1021/acs.chemmater.3c00801
Chem. Mater. XXXX, XXX, XXX−XXX

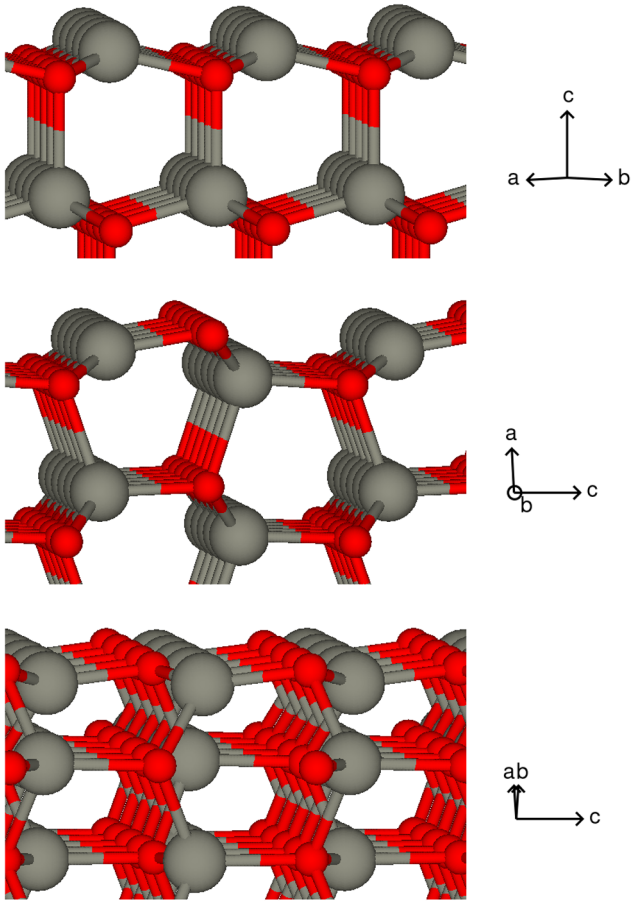

Figure 1. Ball-and-stick representations of some low-index ZnO surfaces after relaxation. From top to bottom: {0001}, {10$\bar{1}$0}, and {11$\bar{2}$0}, respectively.

so no vacuum gap need be included under three-dimensional periodic boundary conditions.) The {10$\bar{1}$0} and {11$\bar{2}$0} surfaces are neutral, Tasker type 1 surfaces,[43] with the surfaces created on each side of a cleavage plane being equivalent. Some polarization occurs on these surfaces when the cleaved structure is relaxed, with surface oxygens moving toward the vacuum. Importantly, the structures retain the equivalence of the surfaces on both sides of the slab so that the polarization does not lead to a dipole potential from one surface of the slab to the other.

Cleavage along an {0001} plane yields inequivalent Zn-terminated and O-terminated surfaces, with the Zn-terminated surfaces illustrated in Figure 1. This is a Tasker type 3 surface and thus not expected to be stable in real crystals.

Slabs of different thicknesses were modeled to investigate the convergence of the surface properties. Consequently, the surface energy of the different surfaces can be calculated, nominally through the formula

$$E_{\text{surface}} = \frac{E^N_{\text{slab}} - NE_{\text{bulk}}}{A} \quad (1)$$

where E^N_{slab} is the energy for a slab of N "layers", E_{bulk} is the energy of an equivalent amount of bulk material as one layer, and A is the area of the slab surface per slab unit cell (including both surfaces). The convergence of E_{surface} with N depends on the details of precisely how the various quantities in eq 1 are defined and calculated.[44] Here we estimate E_{bulk} using the difference between the total energies of the two thickest slabs, which in practice for the ZnO slabs considered gives uncertainty in the third significant digit of the calculated E_{surface}. The resulting surface energies are listed in Table 1.

Table 1. Calculated Surface Energies of Bare ZnO

surface	density (Zn/Å^2)	energy (J/m^2)
{0001}[a]	0.107	1.601
{10$\bar{1}$0}	0.115	0.840
{11$\bar{2}$0}	0.066	0.871

[a]Cleavage energy to make paired O-terminated and Zn-terminated surfaces.

Table 1 includes a value for the {0001} surface. This is not actually a surface energy but the cleavage energy required to split the crystal into a pair of Zn-terminated and O-terminated surfaces. Note that the definition of cleavage energy used here is consistent with the surface energy, being the energy required to form the new surfaces per unit area of the new surface (counting both sides of the cleave), not per unit area of the cleavage plane. Note also that a number of modifications of the {0001} slab can be envisaged to remove the slab dipole, such as reconstructions or including an inversion domain boundary.[45−50] Some of these will be considered in the next section; while thermodynamic methods can be used to study these surfaces,[40−42,51] no attempt was made to determine surface energies from these slabs.

The binding energies calculated for 1s electrons from oxygen ions in the bare, unreconstructed {10$\bar{1}$0} and {11$\bar{2}$0} surface slabs are shown in Figure 2. As discussed above, these binding energies were shifted to yield a bulk oxygen binding energy of 530 eV.

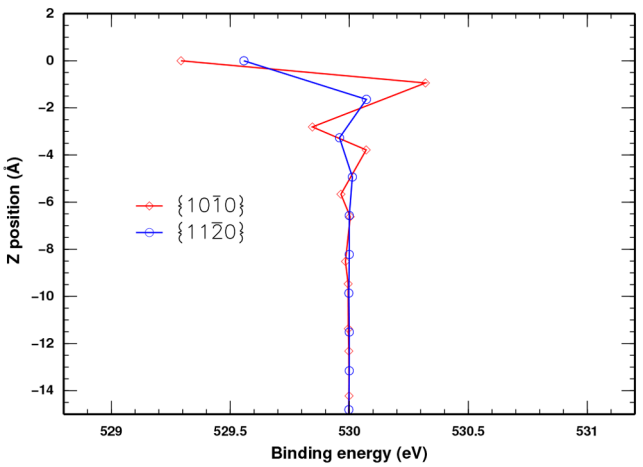

Figure 2. Binding energies of O 1s electrons from different ions in bare ZnO slabs. 1s electrons from bulk oxygen fixed at 530 eV. The Z position (direction normal to the surface) of the oxygen ions on the slab surface is set to zero, with coordinates decreasing into the slab. Lines connecting data points are only to guide the eye.

Only data from the thickest slabs considered are shown in Figure 2. Data from all considered slabs are shown in Figures S2 and S3, which demonstrate the convergence of the calculated O 1s core levels for successively thicker slabs.

Figure 2 demonstrates that pristine {10$\bar{1}$0} and {11$\bar{2}$0} surfaces do not produce an O 1s XPS peak in the vicinity of 531 eV. While some subsurface oxygen ions do exhibit 1s binding energies higher than those of lattice oxygen,[36,37] the largest shifts

https://doi.org/10.1021/acs.chemmater.3c00801
Chem. Mater. XXXX, XXX, XXX−XXX

are for the surface oxygens, which show a binding energy decreased from that of the lattice oxygen by substantially less than 1 eV.

ZnO crystals can form inversion domain boundaries if Sb ions are implanted into the structure.[49] A single computationally expensive slab calculation was performed for a slab with bare O-terminated {0001} surfaces on each face, featuring a 3 × 3 Sb-decorated inversion domain boundary.[49] This slab is not included in Figure 2, but it is included as Figures S4 and S5. The single-relaxed slab calculation indicated that ions in the bare O-terminated {0001} surface yield 1s binding energies lower than those of lattice oxygen, similar to those of the bare {10$\bar{1}$0} and {11$\bar{2}$0} surfaces. Thus, such bare O-terminated {0001} surfaces were not considered further.

3.3. XPS of ZnO Surfaces and Adsorbates. We now turn our attention to calculating the O 1s binding energies for ZnO slabs with some selected surface functionalities. As in the bare slab case described above, we consider only results from the thickest slabs that were studied, for which the differences between the calculated binding energies for ions near the centers and edges of the slabs are deemed to be converged with respect to the thickness of the slabs. The calculated O 1s energy levels for all slabs are shown in the Supporting Information, along with illustrations of the surface structures (Figures S6−S15).

The calculated O 1s binding energies for {10$\bar{1}$0} and {11$\bar{2}$0} slabs with various surface adsorbates are shown in Figure 3. This

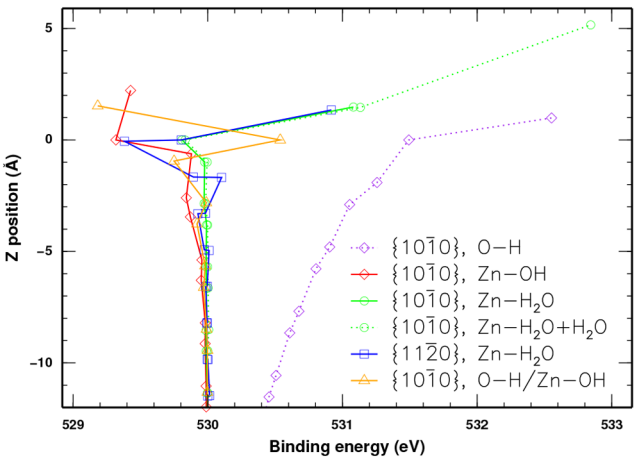

Figure 3. Binding energies of O 1s electrons from different ions in ZnO slabs with different adsorbates. 1s electrons from bulk oxygen fixed at 530 eV. The *Z* position (direction normal to the surface) of oxygen ions on the slab surface is set to zero, with coordinates decreasing in the slab. Lines connecting data points are only to guide the eye.

figure shows that additional OH radical groups attached to the surface ("{10$\bar{1}$0}, Zn-OH") do not significantly alter the binding energy of 1s electrons from the surface oxygen of the ZnO slab (cf. Figure 2) and that the binding energy of 1s electrons from the adsorbed OH oxygen is lower than that of the bulk ZnO lattice oxygen by ∼0.6 eV. The small surface dipole introduced by adsorbed OH radicals slows the absolute convergence of the core electron energy levels (Figure S8), but the difference between the slab center O 1s levels and those of surface and adsorbed oxygen converges quickly with slab thickness.

In contrast, adsorbing a layer of H_2O onto the otherwise clean {10$\bar{1}$0} or {11$\bar{2}$0} surfaces ("{10$\bar{1}$0}, Zn-H_2O" or "{11$\bar{2}$0}, Zn-H_2O", respectively) does impact the binding energy of core electrons of surface oxygen. The surface oxygen of {10$\bar{1}$0} slabs has its core level returned to 0.2 eV below that of lattice oxygen. Half of the surface oxygens of the {11$\bar{2}$0} slab are similarly shifted, while the other half remain at a lower binding energy. Examination of the geometries resulting from relaxation of the structures to their potential energy minimum (Figure 4) shows

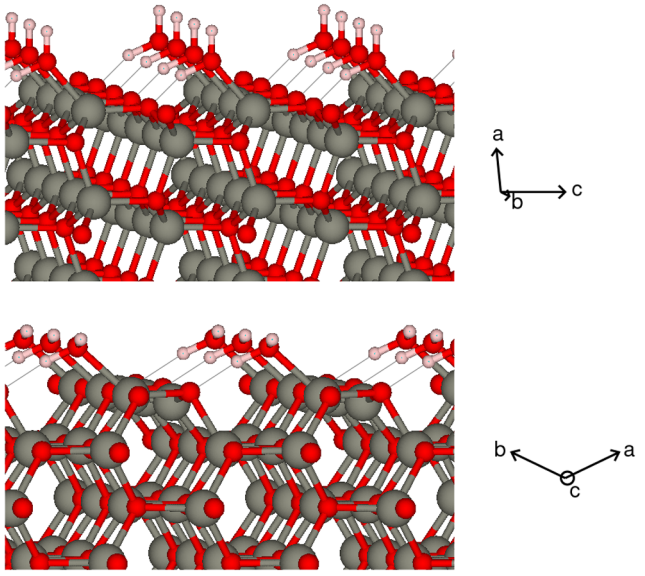

Figure 4. Ball-and-stick representations of {10$\bar{1}$0} (top) and {11$\bar{2}$0} (bottom) ZnO surfaces with water molecules adsorbed. Geometric relaxation from the initial O-down water position used in the DFT calculations rotates the water to form a hydrogen bond with unsaturated surface oxygen.

that this can be explained by apparent hydrogen bonding between the adsorbed molecules and nearby surface oxygen that had been left unsaturated by crystal cleavage. Hydrogen bond acceptors are known to exhibit increased binding energies for core levels.[52] For the {11$\bar{2}$0} surface, only half of the surface oxygen atoms are hydrogen bond acceptors in the considered relaxed structure, leaving half of the calculated surface atom core levels 0.6 eV below that of the lattice oxygen. The water molecules are clearly chemisorbed to the bare ZnO surface through both strong Zn−O interactions and hydrogen bonds.

More importantly, the calculated 1s energy levels of oxygen atoms within adsorbed water on either surface lie ∼1 eV deeper than those of bulk lattice oxygen. These thus correspond to binding energies that are 1 eV larger. This suggests that the commonly observed XPS signal at 531 eV can be explained by O 1s electrons from chemisorbed water.

The O 1s signal of water is usually expected to lie in the vicinity of 533 eV,[53] quite distant from the value of ∼531 eV suggested here. One might be tempted to interpret this as indicating that the core energy level calculation method used here is inaccurate. However, the accuracy of the method can be demonstrated by taking the structure of the {10$\bar{1}$0} slab with water adsorbed on the surface and adding a second water molecule to the cell "above" the adsorbed water, without structural relaxation. The O 1s binding energies from such a calculation are also shown in Figure 3, labeled "{10$\bar{1}$0}, Zn-H_2O +H_2O". The addition of another unbound water to the cell does not significantly alter the core levels of the oxygens of the slab or that of the adsorbed water. The calculated binding energy of the O 1s electrons from the added, weakly interacting water

https://doi.org/10.1021/acs.chemmater.3c00801
Chem. Mater. XXXX, XXX, XXX−XXX

molecule lies at 532.8 eV, consistent with the expected signal from surface-adsorbed (i.e., physisorbed) water molecules.

A similar test is provided by calculating the oxygen core energy levels in slabs with adsorbates containing C−O bonds. The calculated core levels for fully relaxed {10$\bar{1}$0} slabs with adsorbed CO_2 and CHOOH are shown in Figures S17 and S18. The calculated core levels of the oxygens of the adsorbed species lie 1.5−2 eV deeper than those of lattice oxygen, corresponding to these lying in the expected binding energy range of 531.5−532.5 eV.

Adding hydrogen atoms to passivate dangling bonds from surface oxygens ("{10$\bar{1}$0}, O-H" in Figure 3) yields a structure with a surface dipole that does not allow the identification of a convergent core energy that can easily be fixed at 530 eV (Figure S6). Nonetheless, it is notable that attaching hydrogen to the surface oxygen atoms shifts the core energies of those oxygen ions to a level that is just more than 1 eV deeper than those of the oxygen atoms in the slab subsurface. This would suggest that any hydroxides in the surface might be expected to produce an XPS signal in the vicinity of 531 eV.

This was further explored by investigating a structure that might result from partial dissociation of the chemisorbed water considered above (i.e. starting from "{10$\bar{1}$0}, Zn-H_2O"). The hydrogen atom in the physisorbed water molecule that was hydrogen bonded to the surface oxygen is shifted away to allow the hydrogen bond to the surface oxygen to become a covalent bond and break the water O−H bond. The resulting relaxed structure is shown in Figure S15. The calculated O 1s binding energies are labeled "{10$\bar{1}$0}, O-H/Zn-OH" in Figure 3 and show both a significantly higher binding energy for the 1s electrons of the surface oxygen passivated with hydrogen and a lower binding energy for those of the OH bound to Zn. The calculated total energies of the chemisorbed water and dissociatively adsorbed water structures (reflecting the adsorption energy) were not significantly different, although the electron density inside the geometric core region of the attached hydrogen suggests that this configuration yields a more electron poor hydrogen surface species than that observed in "{10$\bar{1}$0}, O-H".

{0001}-dominant surfaces were briefly investigated via the 3 × 3 reconstruction proposed by Jacobs et al.[49] Built on top of a Sb-decorated inversion domain boundary (e.g., Figure S5), this reconstruction reduces the surface dipole through a combination of surface oxygen vacancies and hydrogen adatoms. Calculated oxygen 1s core energy levels for such slabs are shown in Figure S16. Being computationally more expensive due to the larger unit cell, the core energy levels were not fully converged with respect to slab thickness as the slabs that were examined did not indicate that the reconstruction significantly increased the O 1s binding energies above those of the 530 eV lattice oxygens.

We do not explicitly consider slabs with surface vacancies,[3,54] as these would require large surface supercells (making them very computationally expensive), are expected to be Tasker type 3 surfaces (leading to surface dipoles that make slab calculations difficult to converge with respect to slab thickness), and are not expected to directly give higher-binding energy O 1s core electrons.

4. DISCUSSION

Before turning to the interpretation of the XPS spectra, we note that the surface energies listed in Table 1 are well-converged with respect to slab thickness. The values calculated here, starting at 0.84 J/m^2 (0.052 eV/Å^2) for the most stable face, are consistent with the values previously calculated using the PBE functional by Meyer and Marx[40] (noting that they give surface energies per cleaved area, giving values twice that used here) and Liu and Siao.[41] Wander and Harrison[42] have calculated a significantly higher cleavage energy using the B3LYP functional. The work of Na and Park[55] stands out as not only producing higher surface energies but also predicting the {11$\bar{2}$0} surface to be more stable than the {10$\bar{1}$0} surface, contrary to the concensus of this work and the other surface energy determinations.

Many papers have been published that correlate changes in the strength of the XPS signal at 531 eV with changes in observed properties and have leaned on the notion that increased emission corresponding to a binding energy of 531 eV corresponds to an increased bulk oxygen vacancy concentration to link changes in the observed properties to changes in oxygen vacancies.[5−7,9,10,15,16,18,20,23,27,56−60] This work does not support such an interpretation. This leaves the conclusions of a large number of published works subject to revision and reinterpretation.

It is clearly beyond the scope of this work to provide such widespread revision. However, there are several obvious ways that these results can be reinterpreted once it is accepted that the 531 eV XPS signal corresponds to either water chemisorbed with both the O → Zn dative bonding and OH···O hydrogen bonding or surface hydroxides/hydroxyls.

One obvious interpretation is that the changes in the properties that are correlated with changes in the XPS spectrum are actually influenced by surface functionalization. Correlations with photoluminescent and catalytic properties (e.g., refs 10, 20, and 56−58) seem especially simple to reinterpret in this way.

Another obvious interpretation lies in the work of Idriss.[3,54] Idriss emphasizes that unstable oxygen defects on the surfaces of oxides will be quickly "healed" by dissociative adsorption of water into any surface vacancies, replacing any missing oxygen ions with OH species and liberating additional hydrogen to bind with other surface oxygens. The 531 eV XPS peak would then be generated by surface hydroxyls, which act as a proxy for transient surface oxygen defects. Note that due to the unstable nature of surface vacancies, cation-bonded hydroxides like those present in the "{10$\bar{1}$0}, O-H/Zn-OH" structure would likely also migrate to fill any surface oxygen vacancies to yield structures similar to our "{10$\bar{1}$0}, O-H".

A third interpretation is that the observed changes to properties are indeed correlated with changes to the oxygen vacancy concentration in the material, but it is coincidental that the treatments that are altering the vacancy concentration are also altering the surface functionalization of the material in a way that alters the relative intensity of the XPS emission at 531 eV.

In all of the slab calculations presented here, "unsaturated" oxygen ions in the exposed surface layer of the material exhibited core energy levels significantly shallower than those of lattice oxygen in the interior, bulklike regions of the slabs. In many cases, there was oscillation of core energy levels above and below the lattice oxygen level in the slab subsurface. Such core levels would contribute to broadening the main XPS peak around 530 eV. Nonetheless, much of the calculated variation of the oxygen binding energies is suppressed in slabs in which adsorbants are in geometries where they can donate a hydrogen bond to the surface oxygen. The fact that the main 530 eV O 1s peak is not usually sufficiently broad to extend down to the vicinity of 529

https://doi.org/10.1021/acs.chemmater.3c00801
Chem. Mater. XXXX, XXX, XXX−XXX

eV binding energies suggests that atomically clean ZnO surfaces are rarely obtained for XPS characterization.

5. CONCLUSION

In this work, we have critically examined the notion of oxygen vacancies leading to a distinct XPS peak at a binding energy of 531 eV, ∼1 eV greater than the main O 1s peak at 530 eV. We have done this by explicitly calculating the core energy levels of oxygen ions in ZnO crystals and slabs, from which we can identify the binding energies of electrons expected to be ejected from the O 1s orbitals of particular crystal structures, taking full account of the material-dependent electrostatics and electronic structure imposed by local bonding environments.

Despite considering a range of more or less likely structures containing oxygen defects, we find no evidence that a 531 eV binding energy signal could be caused by oxygen defects in the bulk.

Slab calculations reveal that 531 eV binding energy electrons can result from photoejecting 1s electrons from oxygen atoms within water chemisorbed on the surface of the crystals. This does not contradict the body of evidence that surface water in other systems produces an XPS signal at 533 eV, as we find that more loosely bound water in the same calculations contains core electrons corresponding to a binding energy of 533 eV. Surface oxygen atoms passivated with adsorbed hydrogen may also be a source of 531 eV binding energy photoemission.

■ ASSOCIATED CONTENT

Supporting Information

The Supporting Information is available free of charge at https://pubs.acs.org/doi/10.1021/acs.chemmater.3c00801.

An analysis of the origin of the identification of an XPS signal at 531 eV as oxygen vacancies, all calculated oxygen core level energies, and representitive slab surface structures (PDF)

■ AUTHOR INFORMATION

Corresponding Authors

Terry J. Frankcombe − *School of Science, University of New South Wales, Canberra 2600, Australia*; Email: t.frankcombe@adfa.edu.au

Yun Liu − *Research School of Chemistry, Australian National University, Canberra, ACT 2601, Australia*; Email: yun.liu@anu.edu.au

Complete contact information is available at: https://pubs.acs.org/10.1021/acs.chemmater.3c00801

Notes

The authors declare no competing financial interest.

■ ACKNOWLEDGMENTS

This research was undertaken with the assistance of resources and services from the National Computational Infrastructure (NCI), which is supported by the Australian Government. The authors acknowledge the support of the Australian Research Council (FL210100017 and DP200100159).

■ REFERENCES

(1) XPS is also known as X-ray photoemission spectroscopy (with the same abbreviation) or electron spectroscopy for chemical analysis (ESCA).

(2) Fan, J. C. C.; Goodenough, J. B. X-ray photoemission spectroscopy studies of Sn-doped indium-oxide films. *J. Appl. Phys.* **1977**, *48*, 3524−3531.

(3) Idriss, H. On the wrong assignment of the XPS O1s signal at 531−532 eV attributed to oxygen vacancies in photo- and electro-catalysts for water splitting and other materials applications. *Surf. Sci.* **2021**, *712*, 121894.

(4) Xu, H.; Wei, Z.; Verpoort, F.; Hu, J.; Zhuiykov, S. Nanoscale Au-ZnO Heterostructure Developed by Atomic Layer Deposition Towards Amperometric H_2O_2 Detection. *Nanoscale Res. Lett.* **2020**, *15*, 41.

(5) Chang, F.-M.; Brahma, S.; Huang, J.-H.; Wu, Z.-Z.; Lo, K.-Y. Strong correlation between optical properties and mechanism in deficiency of normalized self-assembly ZnO nanorods. *Sci. Rep.* **2019**, *9*, 905.

(6) Li, S.-S.; Su, Y.-K. Improvement of the performance in Cr-doped ZnO memory devices via control of oxygen defects. *RSC Adv.* **2019**, *9*, 2941−2947.

(7) Alnoor, H.; Savoyant, A.; Liu, X.; Pozina, G.; Willander, M.; Nur, O. An effective low-temperature solution synthesis of Co-doped [0001]-oriented ZnO nanorods. *J. Appl. Phys.* **2017**, *121*, 215102.

(8) Zheng, J. H.; Jiang, Q.; Lian, J. S. Synthesis and optical properties of flower-like ZnO nanorods by thermal evaporation method. *Appl. Surf. Sci.* **2011**, *257*, 5083−5087.

(9) Lee, J.; Chung, J.; Lim, S. Improvement of optical properties of post-annealed ZnO nanorods. *Phys. E* **2010**, *42*, 2143−2146.

(10) Wang, Z.G.; Zu, X.T.; Zhu, S.; Wang, L.M. Green luminescence originates from surface defects in ZnO nanoparticles. *Phys. E* **2006**, *35*, 199−202.

(11) Kazmi, J.; Ooi, P. C.; Goh, B. T.; Lee, M. K.; Razip Wee, M. F. Md.; Shafura A Karim, S.; Ali Raza, S. R.; Mohamed, M. A. Bi-doping improves the magnetic properties of zinc oxide nanowires. *RSC Adv.* **2020**, *10*, 23297−23311.

(12) Claros, M.; Setka, M.; Jimenez, Y. P.; Vallejos, S. AACVD Synthesis and Characterization of Iron and Copper Oxides Modified ZnO Structured Films. *Nanomat.* **2020**, *10*, 471.

(13) Wang, J.; Li, Y.; Kong, Y.; Zhou, J.; Wu, J.; Wu, X.; Qin, W.; Jiao, Z.; Jiang, L. Non-fluorinated superhydrophobic and micro/nano hierarchical Al doped ZnO film: the effect of Al doping on morphological and hydrophobic properties. *RSC Adv.* **2015**, *5*, 81024−81029.

(14) Zhang, X.; Qin, J.; Xue, Y.; Yu, P.; Zhang, B.; Wang, L.; Liu, R. Effect of aspect ratio and surface defects on the photocatalytic activity of ZnO nanorods. *Sci. Rep.* **2014**, *4*, 4596.

(15) Shi, S.; Xu, J.; Zhang, X.; Li, L. Effect of annealing on the structural and luminescent properties of ZnO nanorod arrays grown at low temperature. *J. Appl. Phys.* **2011**, *109*, 103508.

(16) Das, J.; Pradhan, S. K.; Sahu, D. R.; Mishra, D. K.; Sarangi, S. N.; Nayak, B. B.; Verma, S.; Roul, B. K. Micro-Raman and XPS studies of pure ZnO ceramics. *Phys. B* **2010**, *405*, 2492−2497.

(17) Han, X.-G.; He, H.-Z.; Kuang, Q.; Zhou, X.; Zhang, X.-H.; Xu, T.; Xie, Z.-X.; Zheng, L.-S. Controlling Morphologies and Tuning the Related Properties of Nano/Microstructured ZnO Crystallites. *J. Phys. Chem. C* **2009**, *113*, 584−589.

(18) Wang, H.; Xie, C. The effects of oxygen partial pressure on the microstructures and photocatalytic property of ZnO nanoparticles. *Phys. E* **2008**, *40*, 2724−2729.

(19) Wang, H.; Baek, S.; Song, J.; Lee, J.; Lim, S. Microstructural and optical characteristics of solution-grown Ga-doped ZnO nanorod arrays. *Nanotech.* **2008**, *19*, 075607.

(20) Hsieh, P.-T.; Chen, Y.-C.; Kao, K.-S.; Wang, C.-M. Luminescence mechanism of ZnO thin film investigated by XPS measurement. *Appl. Phys. A: Mater. Sci. Process.* **2007**, *90*, 317−321.

(21) Baek, S.; Song, J.; Lim, S. Improvement of the optical properties of ZnO nanorods by Fe doping. *Phys. B* **2007**, *399*, 101−104.

(22) Park, S.-M.; Ikegami, T.; Ebihara, K. Effects of substrate temperature on the properties of Ga-doped ZnO by pulsed laser deposition. *Thin Solid Films* **2006**, *513*, 90−94.

(23) Tam, K. H.; Cheung, C. K.; Leung, Y. H.; Djurišić, A. B.; Ling, C. C.; Beling, C. D.; Fung, S.; Kwok, W. M.; Chan, W. K.; Phillips, D. L.;

Ding, L.; Ge, W. K. Defects in ZnO Nanorods Prepared by a Hydrothermal Method. *J. Phys. Chem. B* **2006**, *110*, 20865−20871.
(24) Ramgir, N. S.; Late, D. J.; Bhise, A. B.; More, M. A.; Mulla, I. S.; Joag, D. S.; Vijayamohanan, K. ZnO Multipods, Submicron Wires, and Spherical Structures and Their Unique Field Emission Behavior. *J. Phys. Chem. B* **2006**, *110*, 18236−18242.
(25) Ye, J. D.; Gu, S. L.; Qin, F.; Zhu, S. M.; Liu, S. M.; Zhou, X.; Liu, W.; Hu, L. Q.; Zhang, R.; Shi, Y.; Zheng, Y. D.; Ye, Y. D. MOCVD growth and properties of ZnO films using dimethylzinc and oxygen. *Appl. Phys. A: Mater. Sci. Process.* **2005**, *81*, 809−812.
(26) Chen, M.; Wang, X.; Yu, Y. H.; Pei, Z. L.; Bai, X. D.; Sun, C.; Huang, R. F.; Wen, L. S. X-ray photoelectron spectroscopy and auger electron spectroscopy studies of Al-doped ZnO films. *Appl. Surf. Sci.* **2000**, *158*, 134−140.
(27) De la Rosa, E.; Sepúlveda-Guzman, S.; Reeja-Jayan, B.; Torres, A.; Salas, P.; Elizondo, N.; Yacaman, M. J. Controlling the Growth and Luminescence Properties of Well-Faceted ZnO Nanorods. *J. Phys. Chem. C* **2007**, *111*, 8489−8495.
(28) Szörényi, T.; Laude, L. D.; Bertóti, I.; Kántor, Z.; Geretovszky, Z. Excimer laser processing of indium-tin-oxide films: An optical investigation. *J. Appl. Phys.* **1995**, *78*, 6211−6219.
(29) Sanjinés, R.; Rosenfeld, D.; Gozzo, F.; Alméras, P.; Perez, L.; Lévy, F.; Margaritondo, G.; Schreiner, W. H. ESCA Investigation of SnO_x Films Used as Gas Sensors. *Surf. Inter. Anal.* **1994**, *22*, 372−375.
(30) Wimmer, E.; Krakauer, H.; Weinert, M.; Freeman, A. J. Full-potential self-consistent linearized-augmented-plane-wave method for calculating the electronic structure of molecules and surfaces: O_2 molecule. *Phys. Rev. B* **1981**, *24*, 864−875.
(31) Weinert, M.; Wimmer, E.; Freeman, A. J. Total-energy all-electron density functional method for bulk solids and surfaces. *Phys. Rev. B* **1982**, *26*, 4571−4578.
(32) Krakauer, H.; Posternak, M.; Freeman, A. J. Linearized augmented plane-wave method for the electronic band structure of thin films. *Phys. Rev. B* **1979**, *19*, 1706−1719.
(33) Alekseeva, U.; Michalicek, G.; Wortmann, D.; Blügel, S. *Euro-Par 2018: Parallel Processing*; Springer International Publishing: Cham, Switzerland, 2018; pp 735−748.
(34) Winkelmann, M.; Di Napoli, E.; Wortmann, D.; Blügel, S. Solution to the Modified Helmholtz Equation for Arbitrary Periodic Charge Densities. *Front. Phys.* **2021**, *8*, 618142.
(35) Perdew, J. P.; Burke, K.; Ernzerhof, M. Generalized Gradient Approximation Made Simple. *Phys. Rev. Lett.* **1996**, *77*, 3865−3868.
(36) Egelhoff, W.F. Core-level binding-energy shifts at surfaces and in solids. *Surf. Sci. Rep.* **1987**, *6*, 253−415.
(37) Spanjaard, D.; Guillot, C.; Desjonquères, M.-C.; Tréglia, G.; Lecante, J. Surface core level spectroscopy of transition metals: A new tool for the determination of their surface structure. *Surf. Sci. Rep.* **1985**, *5*, 1−85.
(38) Lizzit, S.; Baraldi, A.; Groso, A.; Reuter, K.; Ganduglia-Pirovano, M. V.; Stampfl, C.; Scheffler, M.; Stichler, M.; Keller, C.; Wurth, W.; Menzel, D. Surface core-level shifts of clean and oxygen-covered Ru(0001). *Phys. Rev. B* **2001**, *63*, 205419.
(39) Bröder, J. High-throughput All-Electron Density Functional Theory Simulations for a Data-driven Chemical Interpretation of X-ray Photoelectron Spectra. Ph.D. Thesis, Forschungszentrum Jülich, Jülich, Germany, 2020.
(40) Meyer, B.; Marx, D. Density-functional study of the structure and stability of ZnO surfaces. *Phys. Rev. B* **2003**, *67*, 035403.
(41) Liu, P.-L.; Siao, Y.-J. Ab initio study on preferred growth of ZnO. *Scripta Mater.* **2011**, *64*, 483−485.
(42) Wander, A.; Harrison, N. M. An ab-initio study of ZnO($11\bar{2}0$). *Surf. Sci.* **2000**, *468*, L851−L855.
(43) Tasker, P. W. The stability of ionic crystal surfaces. *J. Phys. C: Solid State Phys.* **1979**, *12*, 4977−4984.
(44) Frankcombe, T. J.; Løvvik, O. M. The structure and surface energy of $NaAlH_4$: A comparison of DFT methodologies. *J. Phys. Chem. B* **2006**, *110*, 622−630.
(45) Kresse, G.; Dulub, O.; Diebold, U. Competing stabilization mechanism for the polar ZnO(0001)-Zn surface. *Phys. Rev. B* **2003**, *68*, 245409.
(46) Wahl, R.; Lauritsen, J. V.; Besenbacher, F.; Kresse, G. Stabilization mechanism for the polar ZnO(0001)-O surface. *Phys. Rev. B* **2013**, *87*, 085313.
(47) McCoy, M. A.; Grimes, R. W.; Lee, W. E. Inversion domain boundaries in ZnO ceramics. *J. Mater. Res.* **1996**, *11*, 2009−2019.
(48) Yankovich, A. B.; Puchala, B.; Wang, F.; Seo, J.-H.; Morgan, D.; Wang, X.; Ma, Z.; Kvit, A. V.; Voyles, P. M. Stable p-Type Conduction from Sb-Decorated Head-to-Head Basal Plane Inversion Domain Boundaries in ZnO Nanowires. *Nano Lett.* **2012**, *12*, 1311−1316.
(49) Jacobs, R.; Zheng, B.; Puchala, B.; Voyles, P. M.; Yankovich, A. B.; Morgan, D. Counterintuitive Reconstruction of the Polar O-Terminated ZnO Surface with Zinc Vacancies and Hydrogen. *J. Phys. Chem. Lett.* **2016**, *7*, 4483−4487.
(50) Rečnik, A.; Daneu, N.; Walther, T.; Mader, W. Structure and Chemistry of Basal-Plane Inversion Boundaries in Antimony Oxide-Doped Zinc Oxide. *J. Am. Ceram. Soc.* **2001**, *84*, 2657−2668.
(51) Meyer, B. First-principles study of the polar O-terminated ZnO surface in thermodynamic equilibrium with oxygen and hydrogen. *Phys. Rev. B* **2004**, *69*, 045416.
(52) Kerber, S. J.; Bruckner, J. J.; Wozniak, K.; Seal, S.; Hardcastle, S.; Barr, T. L. The nature of hydrogen in x-ray photoelectron spectroscopy: General patterns from hydroxides to hydrogen bonding. *J. Vac. Sci. Teach. A* **1996**, *14*, 1314−1320.
(53) Henderson, M. A. The interaction of water with solid surfaces: fundamental aspects revisited. *Surf. Sci. Rep.* **2002**, *46*, 1−308.
(54) Idriss, H. Oxygen vacancies role in thermally driven and photon driven catalytic reactions. *Chem Catal.* **2022**, *2*, 1549−1560.
(55) Na, S.-H.; Park, C.-H. First-Principles Study of the Surface of Wurtzite ZnO and ZnS - Implications for Nanostructure Formation. *J. Korean Phys. Soc.* **2009**, *54*, 867−872.
(56) Wei, X. Q.; Man, B. Y.; Liu, M.; Xue, C. S.; Zhuang, H. Z.; Yang, C. Blue luminescent centers and microstructural evaluation by XPS and Raman in ZnO thin films annealed in vacuum, N_2 and O_2. *Phys. B* **2007**, *388*, 145−152.
(57) Fan, H.-B.; Yang, S.-Y.; Zhang, P.-F.; Wei, H.-Y.; Liu, X.-L.; Jiao, C.-M.; Zhu, Q.-S.; Chen, Y.-H.; Wang, Z.-G. Investigation of oxygen vacancy and internstitial oxygen defects in ZnO films by photoluminescence and X-ray photoelectron spectroscopy. *Chin. Phys. Lett.* **2007**, *24*, 2108−2111.
(58) Tang, Y.; Zhou, H.; Zhang, K.; Ding, J.; Fan, T.; Zhang, D. Visible-light-active ZnO via oxygen vacancy manipulation for efficient formaldehyde photodegradation. *Chem. Eng. J.* **2015**, *262*, 260−267.
(59) Li, X.; Wang, Y.; Liu, W.; Jiang, G.; Zhu, C. Study of oxygen vacancies' influence on the lattice parameter in ZnO thin film. *Mater. Lett.* **2012**, *85*, 25−28.
(60) Wang, J.; Wang, Z.; Huang, B.; Ma, Y.; Liu, Y.; Qin, X.; Zhang, X.; Dai, Y. Oxygen Vacancy Induced Band-Gap Narrowing and Enhanced Visible Light Photocatalytic Activity of ZnO. *ACS Appl. Mater. Interfaces* **2012**, *4*, 4024−4030.

https://doi.org/10.1021/acs.chemmater.3c00801
Chem. Mater. XXXX, XXX, XXX−XXX